Journal of Power Sources 182 (2008) 153–159

Contents lists available at ScienceDirect

Journal of Power Sources

journal homepage: www.elsevier.com/locate/jpowsour

A mechanical–electrical finite element method model for predicting contact resistance between bipolar plate and gas diffusion layer in PEM fuel cells

Xinmin Lai[a,*], Dong'an Liu[a], Linfa Peng[a], Jun Ni[b]

[a] State Key Laboratory of Mechanical System and Vibration, Shanghai Jiao Tong University, 800 Dongchuan Road, Shanghai 200240, China
[b] Department of Mechanical Engineering, University of Michigan, Ann Arbor, MI 48109-2125, USA

ARTICLE INFO

Article history:
Received 10 January 2008
Received in revised form 25 March 2008
Accepted 26 March 2008
Available online 1 April 2008

Keywords:
PEM fuel cells
Contact resistance
FEM analysis
Mechanical–electrical

ABSTRACT

Contact resistance between the bipolar plate (BPP) and the gas diffusion layer (GDL) plays a significant role on the power loss in a proton exchange membrane (PEM) fuel cell. There are two types of contact behavior at the interface of the BPP and GDL, which are the mechanical one and the electrical one. Furthermore, the electrical contact behavior is dependent on the mechanical one. Thus, prediction of the contact resistance is a coupled mechanical–electrical problem. The current FEM models for contact resistance estimation can only simulate the mechanical contact behavior and moreover they are based on the assumption that the contact surface is equipotential, which is not the case in a real BPP/GDL assembly due to the round corner and margin of the BPP.

In this study, a mechanical–electrical FEM model was developed to predict the contact resistance between the BPP and GDL based on the experimental interfacial contact resistivity. At first, the interfacial contact resistivity was obtained by experimentally measuring the contact resistance between the GDL and a flat graphite plate of the same material and processing conditions as the BPP. Then, with the interfacial contact resistivity, the mechanical and electrical contact behaviors were defined and the potential distribution of the BPP/GDL assembly was analyzed using the mechanical–electrical FEM model. At last, the contact resistance was calculated according to the potential drop and the current of the contact surface. The numerical results were validated by comparing with those of the model reported previously. The influence of the round corner of the BPP on the contact resistance was also studied and it is found that there exists an optimal round corner that can minimize the contact resistance. This model is beneficial in understanding the mechanical and electrical contact behaviors between the BPP and GDL, and can be used to predict the contact resistance in a new BPP/GDL assembly.

1. Introduction

Fuel cells are considered to be a promising power technology due to their zero pollution and high efficiency [1]. Particularly, the proton exchange membrane (PEM) fuel cells have received broad attentions because of their low-temperature operation, high power density and quick startup. One of the key factors that cause power loss in PEM fuel cells is the contact resistance between the bipolar plate (BPP) and the gas diffusion layer (GDL), especially when stainless steel, titanium or molded graphite is used as the BPP material [2–4]. Contact resistance is determined by the material properties, surface topology, clamping pressure and operation conditions [5]. A high clamping pressure leads to an increase in the contact area between BPP and GDL, which in turn decreases the contact resistance. However, a large pressure may cause GDL to be over compressed which results in flow resistance increasing. Furthermore, a large pressure may deform the MEA causing cell leakage and internal short. Thus, it is important to investigate the contact behavior between BPP and GDL [5–7].

Several theoretical models for predicting the interfacial contact resistance have been reported. Greenwood and Williamson (G&W) statistical model is most recognized nowadays, which is based on the Hertz elastic contact theory [8,9]. Cooper et al. introduced a model (CMY) first in 1969, in which they assumed the surfaces in contact are isotropic and the contact spots are circular [10]. Majumdar et al. developed a fractal model based on a fractal representation of the surfaces [11–13]. In a recent work, Zhou et al. [5] proposed a micro-scale numerical model to predict the contact resistance between BPP and GDL. In their study, BPP surface roughness was simulated and GDL was modeled as randomly distributed fibers with estimated total fiber length. All these models mentioned above rely on the surface roughness of contact bodies, which is limited by resolution setting of the profilometer device [6].

* Corresponding author. Tel.: +86 21 34206303; fax: +86 21 34204542.
E-mail addresses: xmlai@sjtu.edu.cn (X. Lai), daliu@sjtu.edu.cn (D. Liu), penglinfa@sjtu.edu.cn (L. Peng), junni@umich.edu (J. Ni).

0378-7753/$ – see front matter © 2008 Elsevier B.V. All rights reserved.
doi:10.1016/j.jpowsour.2008.03.069

Experimental researches and FEM models on the contact resistance have been reported in the following literatures. Wang et al. [4] studied the contact resistances between carbon paper and different stainless steels and found that 349™ is the best candidate for the PEM fuel cells. Mishra et al. [6] conducted experiments to show the effects of different GDL materials and contact pressure on the electrical contact resistance. Ihonen et al. [14] developed a novel PEM fuel cell assembly to measure the clamping pressure and contact resistances simultaneously. Lee et al. [15] conducted experiments to measure the PEM fuel cell performance on different types of GDL and found that each type of GDL has its own optimal clamping pressure. Chang et al. [16] measured contact resistance between BPP and GDL using a specially designed test rig under various clamping pressure levels. The results also showed that there should be a trade-off of the clamping pressure to optimize the contact resistance and mass transfer. Ge et al. [17] studied the effects of GDL compression on fuel cell performance using a unique fuel cell test fixture. Lee et al. [18] proposed a FEM model and analyzed the MEA pressure distribution under given assembly pressure in a single cell. Zhou et al. [19] developed a FEM model to analyze the ohmic contact resistance between the BPP and the GDL, the GDL deformation, and the GDL porosity distribution.

Nevertheless, the electrical contact resistance is a parameter of electrical field while the contact pressure has to be obtained by a mechanical analysis. Moreover, the electrical contact resistance is dependent on the contact pressure. Thus, prediction of the electrical contact resistance is a coupled mechanical–electrical problem. It was attempted in the past to decouple the solution. For example, Zhou et al. [20] and Zhang et al. [21] developed mechanical FEM models to first obtain the contact pressure and the contact area for each contact element, and then calculate the contact resistance based on a contact resistance–pressure constitutive relation. In their FEM models, the contact resistance is calculated based on the assumptions that the contact surface is equipotential and the electric circuit of the contact surface is in a parallel connection. However, in a real BPP/GDL assembly, due to the round corner and the margin of the BPP, there are potential variances on the contact surface and the electric circuit cannot be treated as parallel simply. Therefore, the precision of their methodology is influenced by these assumptions. In addition, their models cannot simulate the electrical field on the contact surface and obtaining the contact pressure and contact area for each contact element is rather complicated.

In this study, a direct coupled mechanical–electrical FEM model, which can simulate the mechanical and electrical fields simultaneously, was developed to predict the contact resistance between the BPP and the GDL. At first, experiments were conducted to obtain the interfacial contact resistivity between the GDL and a flat graphite plate. Then, with the interfacial contact resistivity, the mechanical–electrical FEM model for a real 2D BPP/GDL assembly was established. At last, the contact resistance was calculated based on the numerical results of the electrical field of the model. The influence of the round corner of BPP on the contact resistance was also studied using the model.

2. Methodology

The main purpose of this study is to develop a mechanical–electrical FEM model to predict the contact resistance between the BPP and GDL. The schematic of the methodology is shown in Fig. 1, which consists of two steps.

- *Step 1: acquirement of the interfacial contact resistivity by experiment*. Two experimental setups were built to obtain the interfacial contact resistivity between the GDL and the flat graphite plate of the same material and processing conditions as the BPP. The first experimental setup is conducted with the GDL sandwiched between two flat graphite plates. The second experimental setup is similar but with only one flat graphite plate and no GDL. Then, based on the experimental results, the interfacial contact resistance between the flat graphite plate and the GDL is obtained. At last, the interfacial contact resistivity is calculated according to the interfacial contact resistance and the contact area.
- *Step 2: numerical modeling process for the mechanical–electrical FEM model*. The well-established mechanical–electrical finite element method was developed for the numerical model. At first, the geometry parameters were collected from a practical BPP/GDL assembly to conduct the CAD model. Then, the material properties are the same with those of the experiments in step 1. Meshing is also important to obtain an accurate result. The significant difference in thickness between the BPP and the GDL requires a special consideration in the meshing scheme. The loading and boundary conditions, and the behavior of the contacting interface must be consistent with the actual physical situation. There are two types of contact behavior at the interface, which are the mechanical one and the electrical one, and the latter is dependent on the former. The relationship between the mechanical and the electrical contact behaviors is defined with the interfacial contact resistivity obtained in step 1 as shown in Fig. 1.

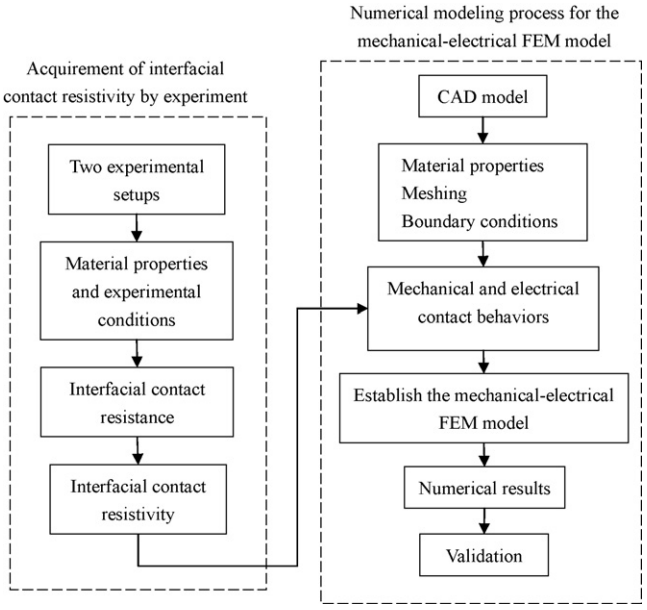

Fig. 1. Schematic of the methodology of the mechanical–electrical FEM model.

After the two contact behaviors were defined, the mechanical–electrical FEM model is established. Executing the model under a set of clamping pressures, the relationship between the contact resistance and the clamping pressure is obtained. After the validation, the developed numerical model can be used to predict the contact resistance in a new BPP/GDL assembly and/or optimize the BPP geometry.

3. Mechanical–electrical FEM model for a real 2D BPP/GDL assembly

According to the methodology in Section 2, a mechanical–electrical FEM model for a real 2D BPP/GDL assembly was developed to predict the contact resistance between the BPP and GDL.

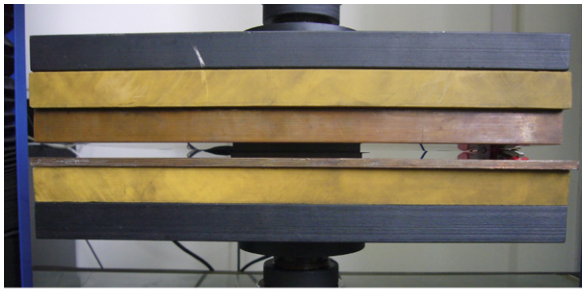

(a)

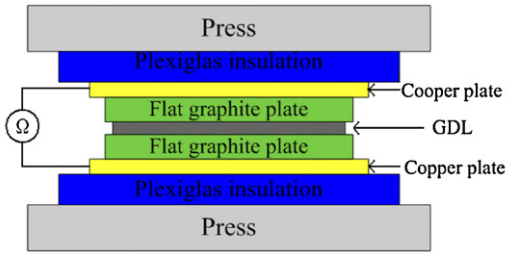

(b)

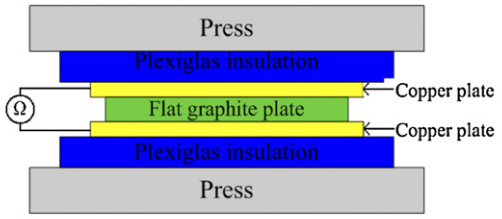

(c)

Fig. 2. (a) Photograph and (b and c) schematics of the two experimental setups.

3.1. Acquirement of the interfacial contact resistivity by experiment

3.1.1. Two experimental setups

Experimental investigations were conducted to obtain the interfacial electrical property. Two experimental setups were built to measure the contact resistance between the GDL and a flat graphite plate of the same material and processing conditions as the BPP [6,21]. A photograph and schematics of the two experimental setups are shown in Fig. 2(a)–(c), respectively.

As shown in Fig. 2(a) and (b), setup 1 consists of a KQL hydraulic press with a load capacity of 100 kN, a pair of Plexiglas plate, a ZY9858 milliohm meter with a resolution of 0.1 μΩ and two copper plates. The GDL was sandwiched between two flat graphite plates of the same material and processing conditions as the BPP. Then, the sandwiched BPP/GDL assembly was placed between the two copper plates. To insulate the electrical circuit from the press, a pair of Plexiglas plate was placed between the press and the copper plate. Kelvin clip leads were used to connect the cooper plate to the milliohm meter. The milliohm meter was used to measure the total resistance of the whole setup. Another similar setup 2 was also built with only one flat graphite plate between the two copper plates as shown in Fig. 2(c).

3.1.2. Material properties and experimental conditions

The GDL for the experiments is Toray TGP-H-060 from Toray Industries, Inc. and the flat graphite plates are supplied by Shanghai Hongfeng Graphite Products Co., Ltd. The mechanical–electrical material properties of the GDL and graphite plate are listed in Tables 1 and 2, respectively. Since the bulk resistances of the GDL and the graphite plates are quite small, they were treated to be independent of the compressive pressure [5,21].

Table 1
Mechanical–electrical properties of TGP-H-060 GDL

Properties (units)	Value
Bulk density (g cm^{-3})	0.44
Porosity (%)	78
Electrical resistivity (mΩ cm)	
Through plane	80
In plane	5.8
Flexural strength (MPa)	40
Tensile strength (N cm^{-1})	50
Young's modulus (MPa)	6.1
Poisson's ratio	0.1

In the experiments, a series of clamping pressures from 0.5 to 4 MPa were applied and the corresponding contact resistances were measured. The increase of the clamping pressure is different when it is in different ranges, which is an increase of 0.1 MPa at the range of 0.5–3 and 0.2 MPa at the range of 3–4 MPa. Since the graphite plate and the GDL are flat, the clamping pressure applied on the assembly is equal to the contact pressure at the interface. Under each certain clamping pressure, the contact resistance measurements were repeated five times to obtain the average values.

3.1.3. Interfacial contact resistance and resistivity calculation

As shown in Fig. 2(b), the measured resistance R_{Mea_1} of the experimental setup 1 can be expressed as:

$$R_{\mathrm{Mea}_1} = 2R_{\mathrm{Co/Gr}} + 2R_{\mathrm{Gr}} + 2R_{\mathrm{Gr/GDL}} + R_{\mathrm{GDL}} \quad (1)$$

where $R_{\mathrm{Co/Gr}}$ is the interfacial contact resistance between the copper plate and the flat graphite plate; R_{Gr} is the bulk resistance of the flat graphite plate; $R_{\mathrm{Gr/GDL}}$ is the interfacial contact resistance between the flat graphite plate and the GDL; R_{GDL} is the bulk resistance of the GDL.

Similarly, the measured resistance R_{Mea2} of the experimental setup 2 is:

$$R_{\mathrm{Mea}_2} = 2R_{\mathrm{Co/Gr}} + R_{\mathrm{Gr}} \quad (2)$$

From Eqs. (1) and (2), the interfacial contact resistance $R_{\mathrm{Gr/GDL}}$ between the flat graphite plate and the GDL is calculated as:

$$R_{\mathrm{Gr/GDL}} = \frac{R_{\mathrm{Mea}_1} - R_{\mathrm{Mea}_2} - R_{\mathrm{Gr}} - R_{\mathrm{GDL}}}{2} \quad (3)$$

where R_{Gr} and R_{GDL} were calculated according to the electrical resistivity of the flat graphite plate and GDL, respectively [5,21]. Hence, by measuring R_{Mea_1} and R_{Mea_2} under a series of clamping pressures, a set of $R_{\mathrm{Gr/GDL}}$ were obtained. However, $R_{\mathrm{Gr/GDL}}$, whose unit is mΩ, is the interfacial contact resistance between the flat graphite plate and the GDL, and it changes with the size of the flat graphite plate

Table 2
Mechanical–electrical properties of flat graphite plate

Properties (units)	Value
Thickness (mm)	4
Bulk density (g cm^{-3})	≥1.85
Electrical resistivity (mΩ cm)	
Through plane	1.2
In plane	0.3
Compressive strength (MPa)	105
Yong's modulus (MPa)	120
Poisson's ratio	0.22
Permeability coefficient of air	No air pressure leakage

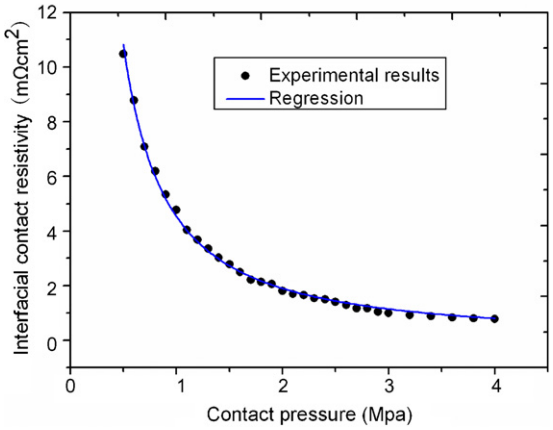

Fig. 3. Relationship between the interfacial contact resistivity and the contact pressure, and the regression result.

and the GDL. Therefore, in order to represent the interfacial electrical property between the graphite plate and the GDL, the interfacial contact resistivity $\rho_{Gr/GDL}$ is defined by [20]:

$$\rho_{Gr/GDL} = R_{Gr/GDL} A_{Gr/GDL} \quad (4)$$

where $A_{Gr/GDL}$ is the contact area between the flat graphite plate and the GDL.

The units of $A_{Gr/GDL}$ and $\rho_{Gr/GDL}$ are cm^2 and $m\Omega\,cm^2$, respectively. Therefore, $\rho_{Gr/GDL}$ is independent of the size of flat graphite plate and the GDL, but only influenced by their material properties and processing conditions. $\rho_{Gr/GDL}$ was used to define the relationship between the mechanical and the electrical contact behavior in the present study as shown in Fig. 3.

3.2. Numerical modeling process for the mechanical–electrical FEM model

In a real PEM fuel cell stack, the contact pressure on the GDL is different from the clamping pressure because of the channels in the BPP. Furthermore, due to the round corners of the BPP, the contact behavior at the interface is hard to predict without a FEM analysis. With the interfacial contact resistivity obtained above, a mechanical–electrical FEM model for a real BPP/GDL assembly was developed to predict the interfacial contact resistance using the commercial code ANSYS.

The geometrical parameters of the model are extracted from a real BPP/GDL assembly, as shown in Table 3 and Fig. 4(a). Because of the symmetry geometry of the BPP/GDL assembly and in order to save computation time, the section of the BPP/GDL assembly was used to build the model. The mechanical–electrical FEM model was developed as follows:

Table 3
Geometry parameters of the 2D BPP/GDL assembly

Parameters	Value (mm)
H_1	3.0
H_2	1.8
H_3	0.19
W_1	2.00
W_2	2.00
R_1	0.20
R_2	0.20
L	11

3.2.1. Material properties and meshing

The mechanical and electrical material properties of the BPP/GDL assembly used in the simulation are the same as those in the experiments as listed in Tables 1 and 2. The 2D-coupled field element PLANE223 with degrees of freedom of mechanical–electrical is used to represent the BPP and GDL. A combination of mapped meshing and automatic meshing is adopted in order to ensure proper element connectivity and a correct aspect radio as shown in Fig. 4(a).

3.2.2. Loading and Boundary conditions

As shown in Fig. 4(a), loading and boundary conditions are applied as following:

- *Mechanical*. Zero displacement at the left boundary of the model due to the symmetry of the structure; zero displacement for the node on the bottom of the GDL; the uniform clamping pressure P on the top of the BPP.
- *Electrical*. Zero potential on the bottom of the GDL; constant current $I = 1$ A on the top of the BPP forced through the assembly.

3.2.3. Definition of the mechanical and electrical contact behaviors

In a real BPP/GDL assembly, there are two types of contact behavior at the interface, which are the mechanical one and the electrical one. In this study, contact elements CONTA172 and TARGE169 are used to create the contact pairs at the interface to model the two contact behaviors. As mentioned above, the electrical contact behavior is dependent on the mechanical one. However, the traditional contact elements CONTA172 and TARGE169 can only model the mechanical but not the electrical contact behavior. Hence there is a need of modification of the traditional contact element to take into account the interaction for electrical contact.

In Section 3.1, the relationship between the mechanical and electrical contact behavior has been experimentally obtained with the interfacial contact resistivity as shown in Fig. 3. Thus, based on this relationship, an electrical parameter – electrical contact conductance (ECC) – is built into the traditional contact element to simulate the electrical contact behavior at the interface. The ECC, which specifies the electrical contact conductance per unit area for the contact surface, is defined as the reciprocal of the interfacial contact resistivity in this study:

$$\mathrm{ECC} = \frac{1}{\rho_{Gr/GDL}} \quad (5)$$

where $\rho_{Gr/GDL}$ is the interfacial contact resistivity obtained from Eq. (4).

Once ECC is defined, the electrical contact behavior at the interface is modeled as

$$J = \mathrm{ECC}(U_t - U_c) \quad (6)$$

where J is the current density at the interface. U_t and U_c are the potentials of the two sides of the interface, respectively [22].

With ECC defined, the electrical contact behavior at the interface is created and a circuit of the BPP/GDL assembly is built as shown in Fig. 4(b).

3.2.4. Contact resistance prediction between the BPP and GDL

After the two contact behaviors are defined, the mechanical–electrical FEM model for the 2D BPP/GDL assembly is established. The contact resistance is calculated according to the potential drop and the current of the contact surface. From Fig. 4(b), the total resistance of the BPP/GDL assembly can be divided into three parts, which are the bulk resistances R_{BPP} of BPP

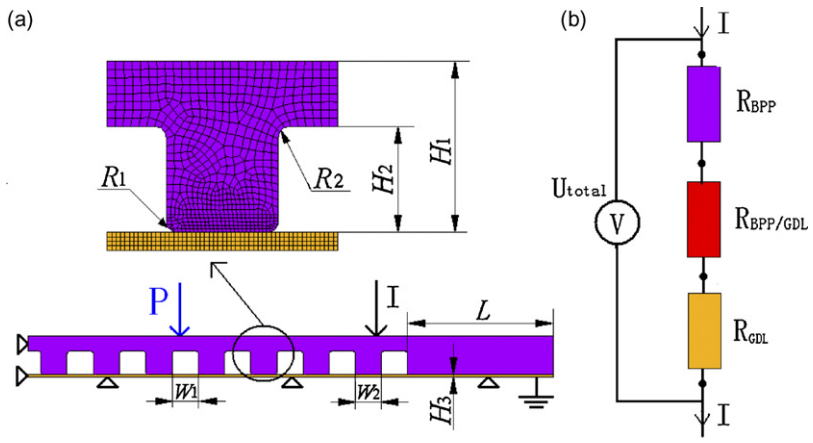

Fig. 4. (a) Geometry parameters and the mechanical–electrical FEM model of the BPP/GDL assembly, and (b) the schematic of the circuit of the assembly.

and R_{GDL} of GDL, and the contact resistance $R_{BPP/GDL}$. According to Ohm's law, the potential drops of the three resistances are

$$U_{BPP} = R_{BPP} \times I; \quad U_{GDL} = R_{GDL} \times I; \quad U_{BPP/GDL} = R_{BPP/GDL} \times I \tag{7}$$

$$U_{total} = U_{BPP} + U_{GDL} + U_{BPP/GDL} \tag{8}$$

where U_{BPP}, U_{GDL}, $U_{BPP/GDL}$ and U_{total} are the potential drops of the BPP, the GDL, the interface and the whole assembly, respectively. Since the current I that passes the interface is a constant, from Eqs. (7) and (8) the contact resistance $R_{BPP/GDL}$ can be calculated as

$$R_{BPP/GDL} = \frac{U_{BPP/GDL}}{I} = \frac{U_{total} - U_{BPP} - U_{GDL}}{I} \tag{9}$$

From Eq. (9), once U_{total}, U_{BPP} and U_{GDL} are obtained using the mechanical–electrical FEM model, $R_{BPP/GDL}$ will be calculated.

Executing the mechanical–electrical FEM model under a range of clamping pressures, the relationship between the contact resistance $R_{BPP/GDL}$ and the clamping pressure P for this 2D BPP/GDL assembly is obtained.

3.3. Validation of the numerical results

As mentioned in Section 1, Ref. [20] developed a mechanical FEM model to predict the contact resistance based on an empirical formula. Although the precision of their model is affected by the assumptions, the general rules revealed by it are proved to be right and can be used to predict the contact resistance. According to Ref. [20], the relationship between the interfacial contact resistivity ρ and the contact pressure P can be defined as:

$$\rho = A\left(\frac{B}{P}\right)^{C} = AB^{C}P^{-C} \tag{10}$$

where A, B and C are parameters determined by experiments.

In this research, Eq. (10) is used to fit the experimental results obtained in Section 3.2 and the regression result shows a pretty good accuracy as shown in Fig. 3. The regression result of this study is:

$$\rho(\mathrm{m\Omega\,cm^2}) = 4.536P^{-1.254} \tag{11}$$

With Eq. (11), the methodology developed by Ref. [20] was implemented on the same 2D BPP/GDL assembly and a set of contact resistance values are obtained. By comparing the two numerical results obtained by the mechanical–electrical FEM model and the methodology of Ref. [20], the validation is conducted.

4. Results and discussions

4.1. Validation results

Numerical results from the mechanical–electrical FEM model and the methodology of Ref. [20] are presented in Fig. 5. The unit of the results is mΩ mm is because it is a 2D model [20]. As Fig. 5 shows, the differences of the two results are in a small range, in particular, when the clamping pressure becomes larger. That is the difference is 1.35 mΩ mm under the clamping pressure of 0.5 MPa and 0.16 mΩ mm of 3 MPa. This is mainly because in the methodology of Ref. [20], calculation of the contact resistance is based on the assumption that the contact surface between the BPP and the GDL is equipotential. However, in a real BPP/GDL assembly, due to the influence of the round corner and the margin of the BPP, there are some variances of the electric potential on the contact surface, especially when the clamping pressure is smaller. Fig. 6 shows the potential distribution on the contact surface under different clamping pressures of 0.5, 1, 2 and 3 MPa. As Fig. 6 shows, the contact surface is not equipotential under each certain clamping pressure and there is potential variance even under a single rib as shown in the enlarged views. Therefore, the equipotential assumption is not quite proper and influences the precision of the methodology of Ref. [20].

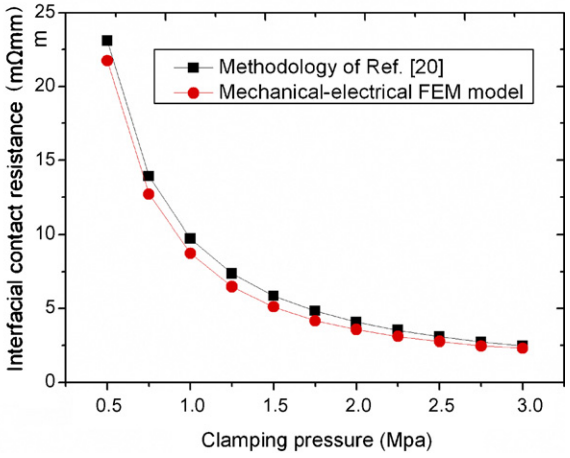

Fig. 5. Comparison of numerical results of the mechanical–electrical FEM model and methodology of Ref. [20].

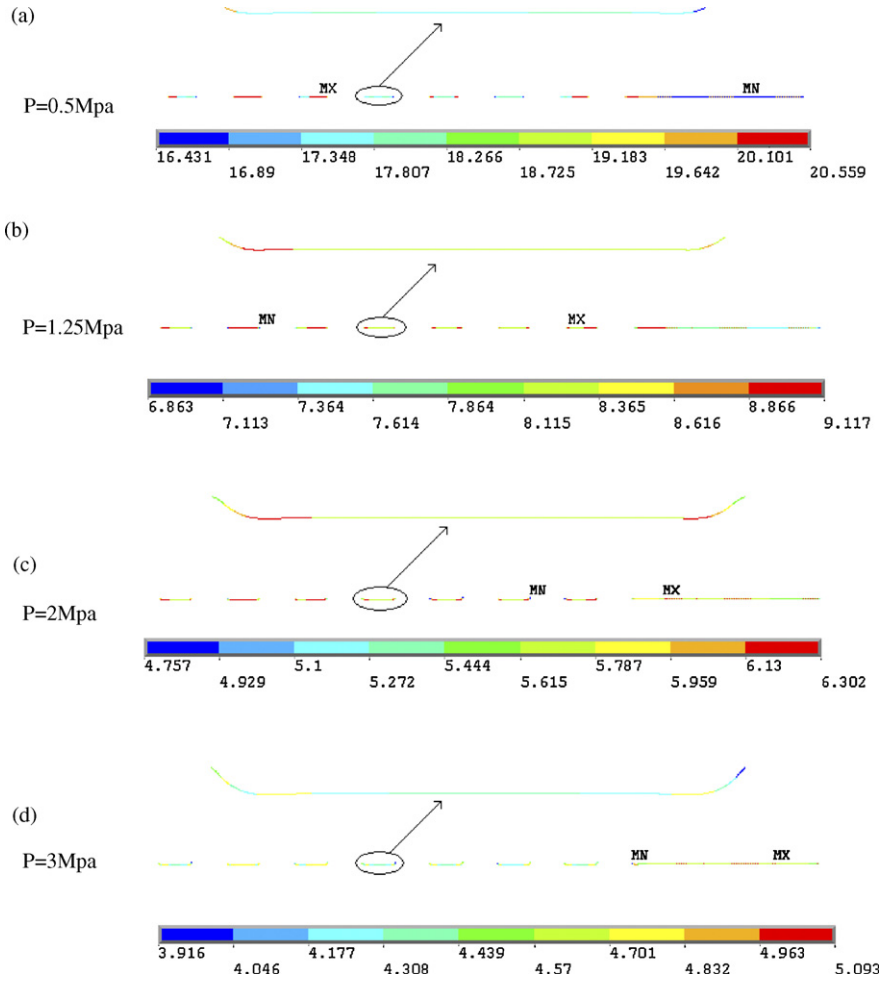

Fig. 6. Contours of the potential distribution on the contact surface under different clamping pressures.

It also can be seen that when the clamping pressure is larger, the potential variance on the contact surface is smaller. That is the maximum potential variance on the contact surface under certain clamping pressure is 4.128 V of 0.5 MPa, 2.254 V of 1.25 MPa, 1.545 V of 2 MPa and 1.177 V of 3 MPa. This means when the clamping pressure becomes larger, the potential variance decreases, which in turn weakens the influences of the assumptions in the methodology of Ref. [20]. Hence when the clamping pressure becomes larger, the two results agree better.

Nevertheless, the two results show the same trend and the maximum difference between them is 6.2% with the clamping pressure of 0.5 MPa. This indicates that the mechanical–electrical FEM model developed in this study reveals the general rules of the contact resistance and represents reasonably well the mechanical and electrical contact behaviors of the BPP/GDL assembly.

4.2. Influence of the round corner on the contact resistance

The round corner of the BPP plays an important role on the contact pressure distribution on the GDL, which in turn influences the contact resistance. Moreover, the round corner has an effect on the potential variance on the contact surface. Thus, the influence of the round corner on the contact resistance is studied using the mechanical–electrical FEM model developed in this study under the typical clamping pressure of 1 MPa in PEM fuel cells.

The round corner R_1 varies at a range of 0.1–0.9 mm with the other parameters kept unchanged as listed in Table 3. The relationship of the contact resistance and the round corner under the clamping pressure of 1 MPa is shown in Fig. 7.

As shown in Fig. 7, the contact resistance first decreases when the round corner R_1 increases from 0.1 to 0.6 mm, but then increases when it increases from 0.6 to 0.9 mm. This is because when the round corner R_1 becomes larger, on the one hand, the contact length between the BPP and GDL is decreased which causes the

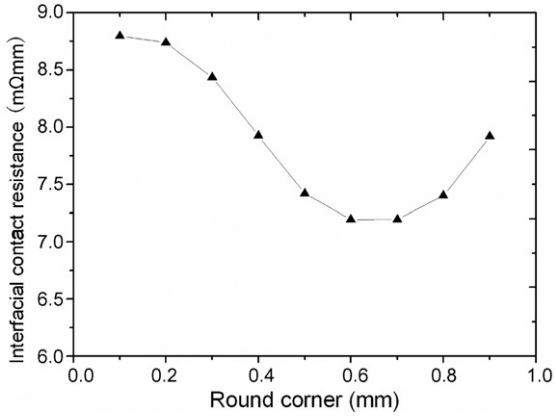

Fig. 7. Influence of the round corner on the contact resistance.

contact resistance to increase, but on the other hand, the contact pressure is increased which results in the decrease of the contact resistance. Therefore, because of the two competitive influences, the contact resistance first decreases and then increases. There is a trade-off between the influences of the contact length and the contact pressure, which makes the contact resistance minimized. Combined with other goals, such as the efficiency and cost, the rib shape can be optimized. Only taking the contact resistance into considered, there is an optimal round corner for this model, which is 0.6 mm.

5. Conclusion

A mechanical–electrical FEM model was developed according to the coupled mechanical–electrical nature of the contact resistance. The model was implemented on a real 2D BPP/GDL assembly based on the experimental interfacial contact resistivity. It proved to be an effective way in predicting the contact resistance of PEM fuel cells. Comparing with the models reported previously of contact resistance estimation, the model proposed in this paper shows the following merits: first, this model is more precise in predicting the contact resistance. The precision of models reported previously is influenced by their assumption, which is the contact surface is equipotential; second, the mechanical–electrical model can simultaneously simulate the mechanical and electrical fields of the BPP/GDL assembly and thus reveals the coupled nature of the contact resistance to the larger extent; third, the model in this study does not need to obtain the contact pressure and contact length for each contact element, which is rather complicated. With the present model, it is simple and effective to calculate the contact resistance according to Ohm's law.

Numerical results of the developed model shows that the contact resistance decreases rapidly as the clamping pressure increases especially when the clamping pressure is in a small value range. The influence of the round corner on the contact resistance was also studied. It is found that with the increase of the round corner, there is a trade-off between the contact length and the contact pressure, which minimizes the contact resistance. Taking only the contact resistance into consideration, the optimal round corner for this study is 0.6 mm.

The model developed in this study is beneficial in understanding the coupled mechanical–electrical nature of the contact behavior between BPP and GDL, and can be applied to predict the contact resistance in a new BPP/GDL assembly and/or to optimize the rib shape of the BPP.

Acknowledgements

The work reported here is sponsored by the National High Technology Research and Development Program of China (20060111A1222). The authors gratefully acknowledge the supports.

References

[1] G. Hoogers, Fuel Cell Technology Handbook, CRC Press, Boca Raton, FL, 2003.
[2] R.C. Makkus, A.H.H. Janssen, F.A. Bruijn, R. Mallant, J. Power Sources 86 (2000) 274–282.
[3] D.P. Davies, P.L. Adcock, M. Turpin, S.J. Rowen, J. Appl. Electrochem. 30 (2000) 101–105.
[4] H.L. Wang, M.A. Sweikart, J.A. Turner, J. Power Sources 115 (2003) 243–251.
[5] Y. Zhou, G. Lin, A.J. Shih, S.J. Hu, J. Power Sources 163 (2007) 777–783.
[6] V. Mishra, F. Yang, R. Pitchumani, ASME J. Fuel Cell Sci. Technol. 1 (2004) 2–9.
[7] P. Zhou, C.W. Wu, G.J. Ma, J. Power Sources 163 (2007) 874–881.
[8] J.A. Greenwood, J.B.P. Williamson, Proc. Roy. Soc. Lond. A 295 (1966) 300–319.
[9] J.A. Greenwood, J.B.P. Williamson, Br. J. Appl. Phys. 17 (1966) 1621–1632.
[10] M.G. Cooper, B.B. Mikic, M.M. Yovanovitch, Int. J. Heat Mass Transfer. 12 (1969) 279–300.
[11] A. Majumdar, C.L. Tien, Wear 136 (1990) 313–327.
[12] A. Majumdar, B. Bhushan, J. Tribol. 112 (1990) 205–216.
[13] A. Majumdar, B. Bhushan, J. Tribol. 113 (1991) 1–11.
[14] J. Ihonen, F. Jaouen, G. Lindbergh, G. Sundholm, Electrochim. Acta 46 (2001) 2899–2911.
[15] W.-K. Lee, C.-H. Ho, J.W. Van Zee, M. Murthy, J. Power Sources 84 (1999) 45–51.
[16] W.R. Chang, J.J. Hwang, F.B. Weng, S.H. Chan, J. Power Sources 166 (2007) 149–154.
[17] J. Ge, A. Higier, H. Liu, J. Power Sources 159 (2006) 922–927.
[18] S.J. Lee, C.D. Hsu, C.H. Huang, J. Power Sources 145 (2005) 353–361.
[19] P. Zhou, C.W. Wu, J. Power Sources 170 (2007) 93–100.
[20] P. Zhou, C.W. Wu, G.J. Ma, J. Power Sources 159 (2006) 1115–1122.
[21] L. Zhang, Y. Liu, H. Song, S. Wang, Y.Y. Zhou, S.J. Hu, J. Power Sources 162 (2006) 1165–1171.
[22] ANSYS. Inc, Modeling Electric Contact, Contact Technology Guide, 2007.